Supporting Information

Bi alloying into rare earth double perovskites enhances synthesizability and visible light absorption

*Paul F. Newhouse[1], Lan Zhou[1], Mitsutaro Umehara[1,2], David A. Boyd[1,3], Edwin Soedarmadji[1], Joel A. Haber[1], John M. Gregoire[1,4]**

[1] Joint Center for Artificial Photosynthesis, California Institute of Technology, Pasadena, CA 91125, United States; [2] Future Mobility Research Department, Toyota Research Institute of North America, Ann Arbor, MI 48105, United States; [3] Division of Physics, Mathematics, and Astronomy, California Institute of Technology, Pasadena, CA 91125, United States; [4] Division of Engineering and Applied Science, California Institute of Technology, Pasadena, CA 91125, United States.

*gregoire@caltech.edu

a

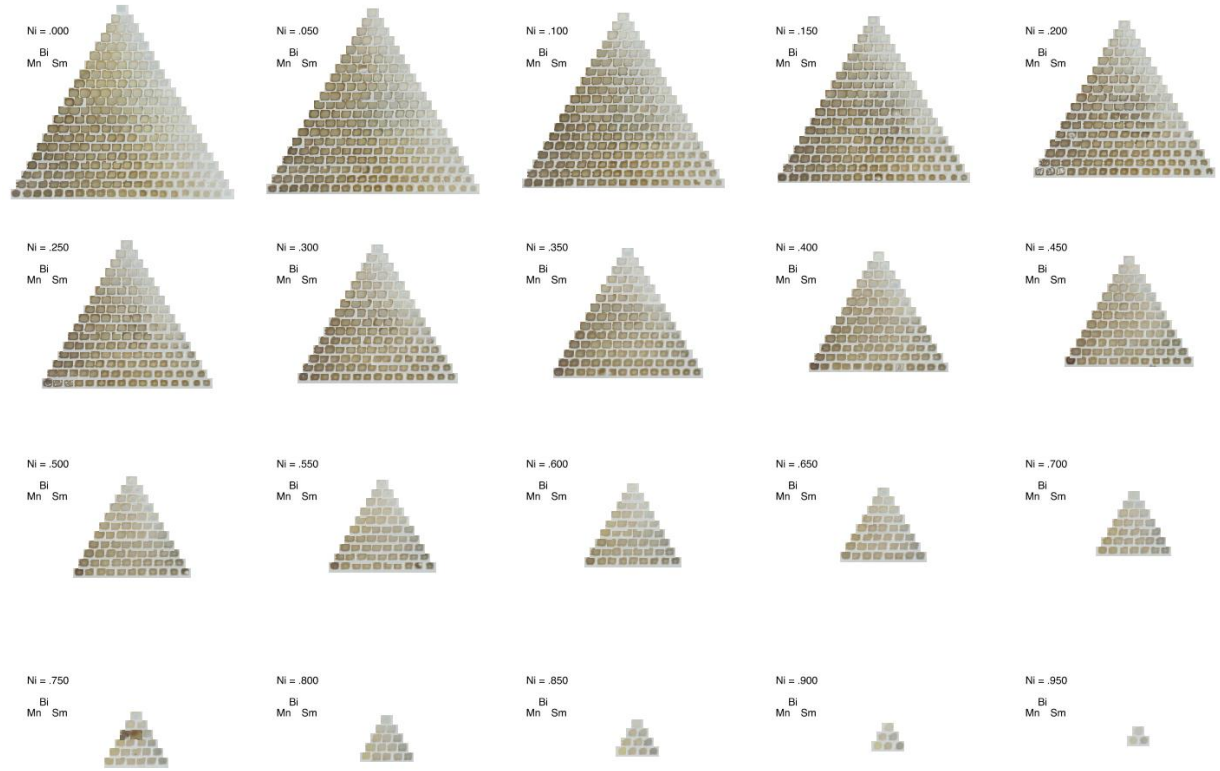
Ni = .000
Ni = .050
Ni = .100
Ni = .150
Ni = .200
Ni = .250
Ni = .300
Ni = .350
Ni = .400
Ni = .450
Ni = .500
Ni = .550
Ni = .600
Ni = .650
Ni = .700
Ni = .750
Ni = .800
Ni = .850
Ni = .900
Ni = .950
Bi
Mn Sm

b

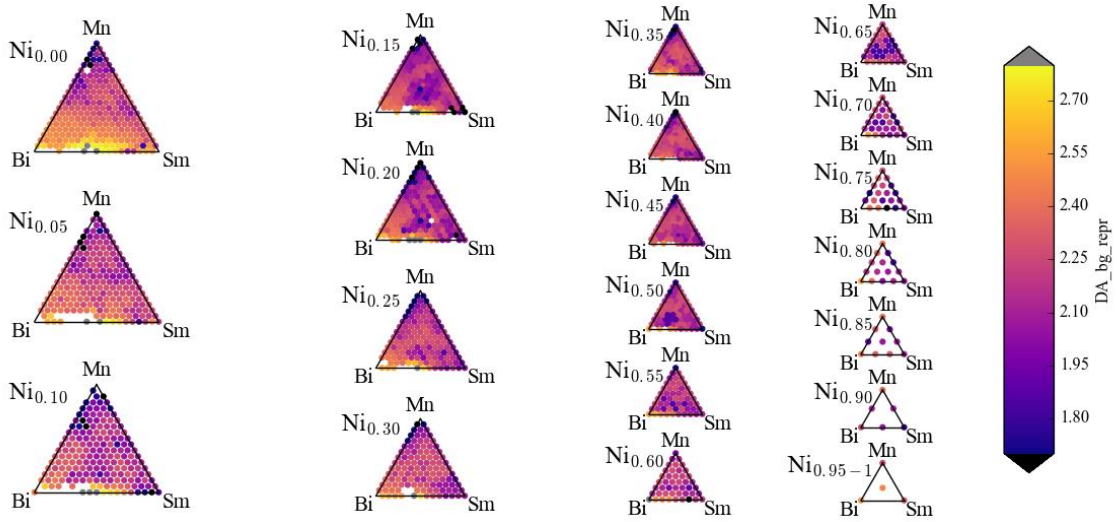
Mn
Ni0.00
Ni0.05
Ni0.10
Ni0.15
Ni0.20
Ni0.25
Ni0.30
Ni0.35
Ni0.40
Ni0.45
Ni0.50
Ni0.55
Ni0.60
Ni0.65
Ni0.70
Ni0.75
Ni0.80
Ni0.85
Ni0.90
Ni0.95 – 1
Bi
Sm
2.70
2.55
2.40
2.25
2.10
1.95
1.80
DA_bg_repr

c

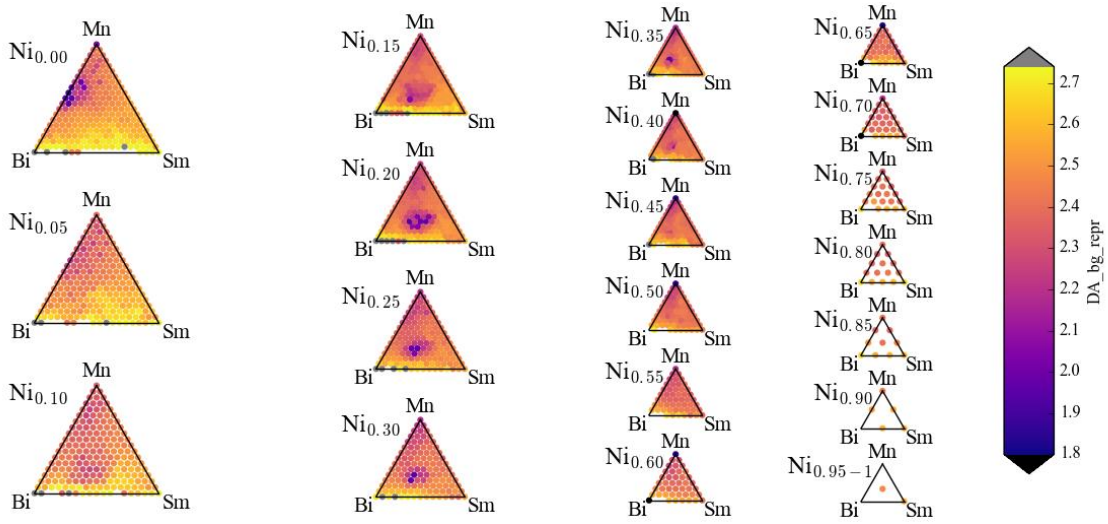

Figure S1(a,b,c). Physical composition space images of a Bi-Mn-Sm-Ni library plate on a-SiO2 substrate (a), and the corresponding direct allowed band gap (b). The direct allowed band gap map for the library plate in Fig.1 on an FTO substrate is shown in (c). The composition-optical trends are similar on the 2 different substrates, with the higher quality of the library on FTO motivating its use for optical analysis in the main text.

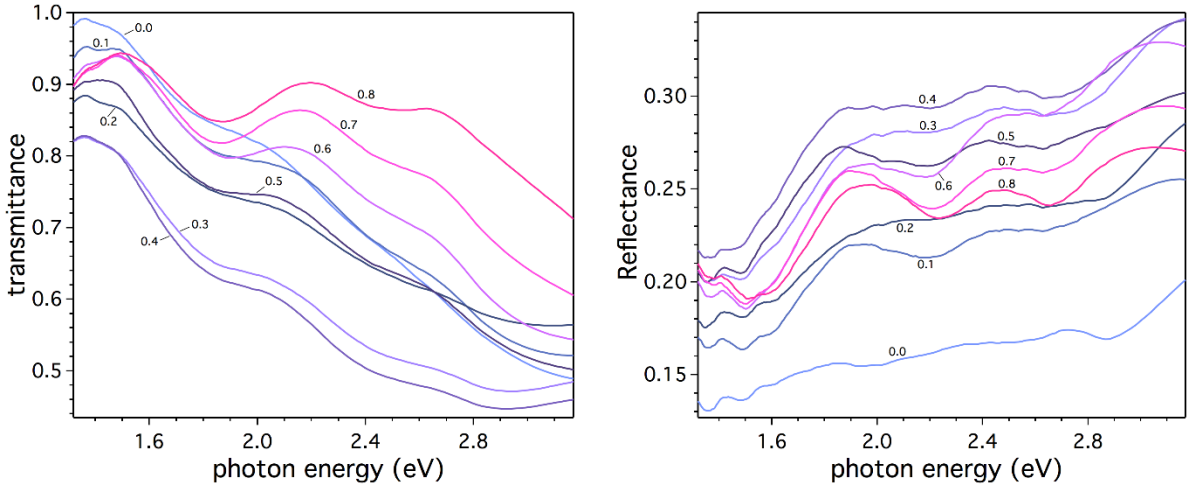

Figure S2. The fractional transmittance (T) and reflectance (R) spectra corresponding to the calculation of optical absorption spectra in Fig. 2a

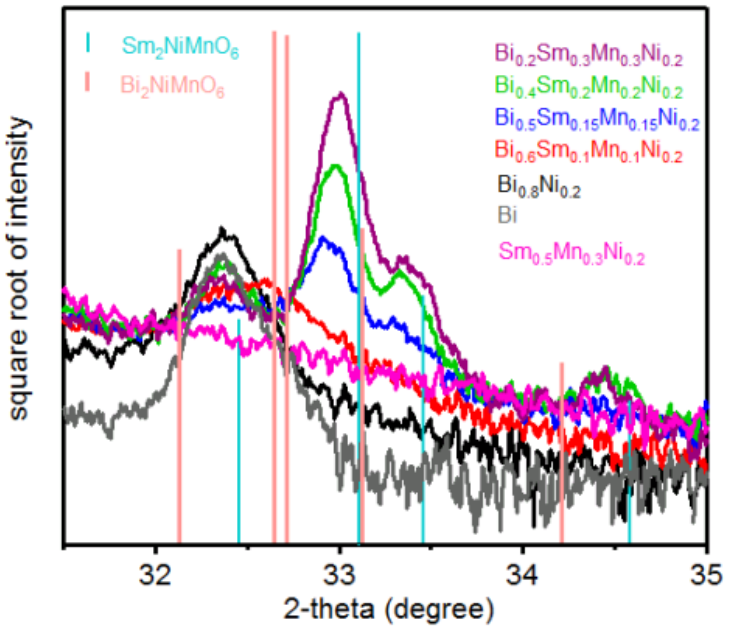

a

Fig. S3. The portion of the XRD patterns from Fig. 3 where peak shifting between the XRD patterns for Sm_2MnNiO_6 and Bi_2MnNiO_6 is most apparent. Considering the relative position from the strongest peak in the Sm end member phase and the average position of the corresponding doublet peak in the Bi end member phase, the peak positions in the XRD patterns for the x = 0.2 to 0.5 samples correspond to an average lattice constant that is 30-50% shifted from that of the Sm phase toward that of the Bi phase, providing the best estimate of the Bi site occupancy from the thin films samples.

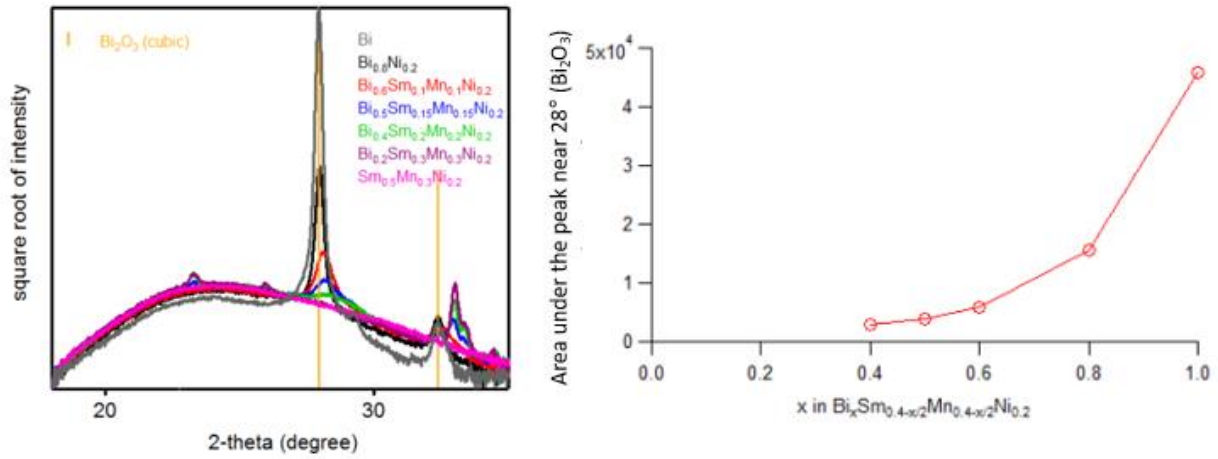

Fig. S4. The portion of the raw XRD measurements (no background subtraction) of the XRD patterns in Fig. 3 in the vicinity of the primary Bi_2O_3 peak. The intensity of this peak as a function of Bi concentration x is shown at the right, where the intensity at x = 0.4 corresponds to a broad feature that by itself would not be recognizable as a Bi_2O_3 peak, suggesting that the onset of crystallization into this structure occurs near this composition.

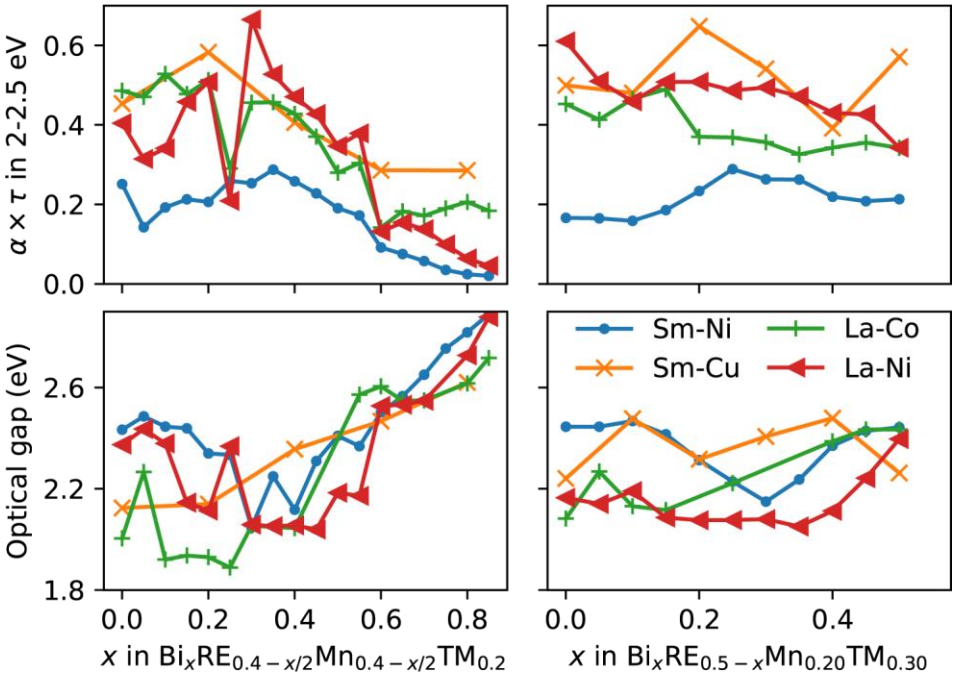

Figure S5. The thickness scaled absorption coefficient $\alpha \times \tau$ and direct allowed optical band gap of 3 additional Bi-Mn-RE-TM libraries as a function of composition spanning two quaternary compositional lines, analogous to Fig. 5. The Sm-Ni line from Fig. 5 is included for comparison. Sm-Cu has fewer data points as this library was synthesized with 10% steps instead of 5% for the others.

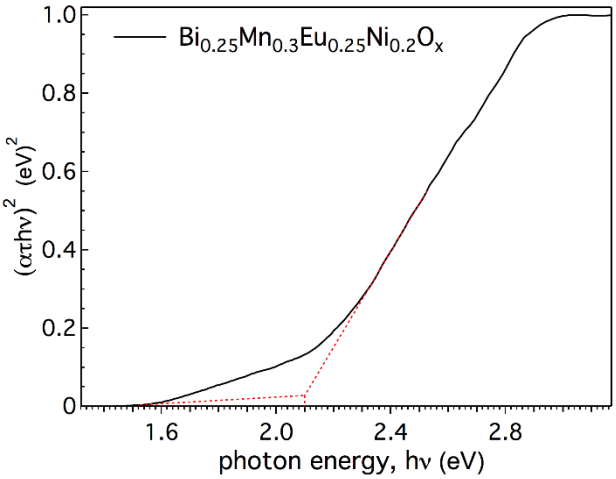

Figure S6. Direct-allowed absorption spectra from a representative Bi-alloyed Eu_2MnNiO_6 double perovskite plotted with dashed linear segments used to extract the band gap value of 2.1 eV (see also Fig. S5b).

a

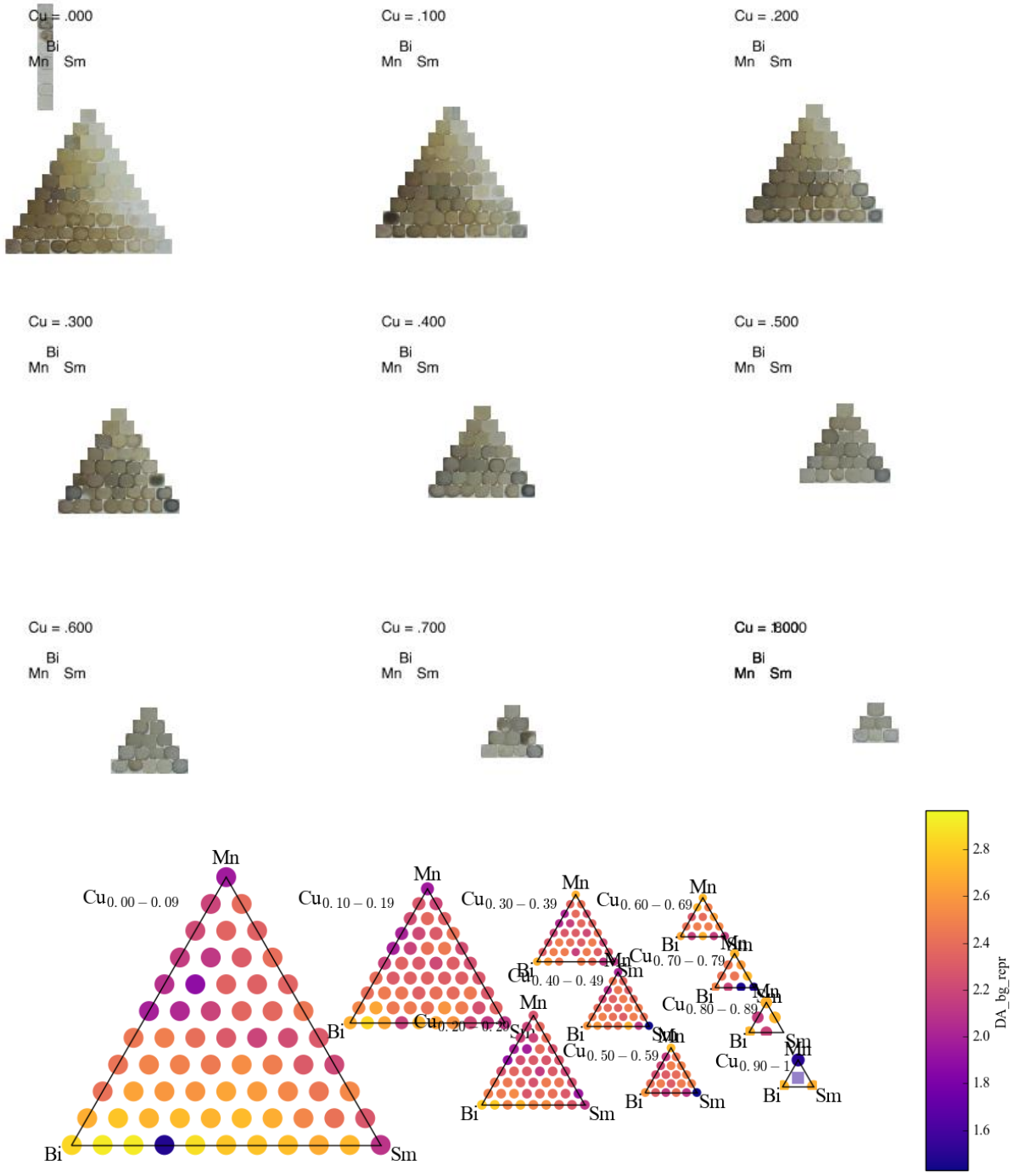

Figure S7(a,b). Physical composition space images (a) and direct allowed band gap (b) of a Bi-Mn-Sm-Cu 10 at.% library of an FTO substrate.

a

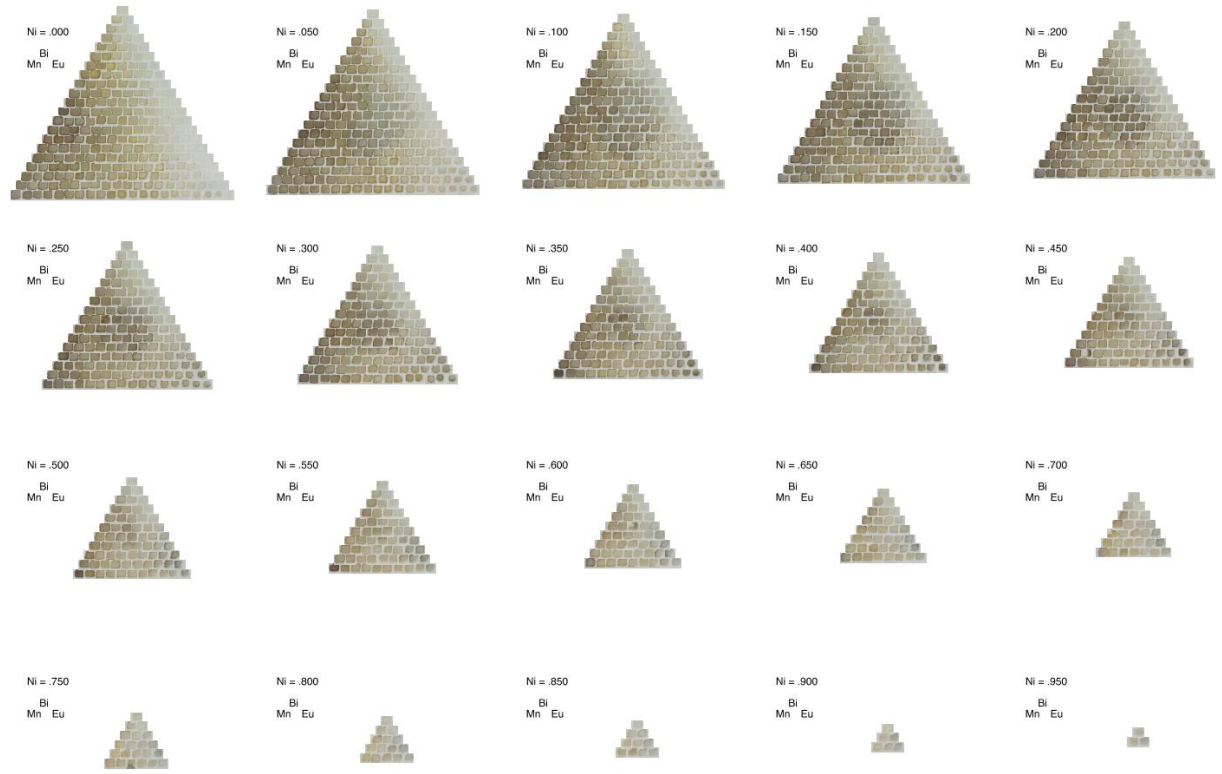

b

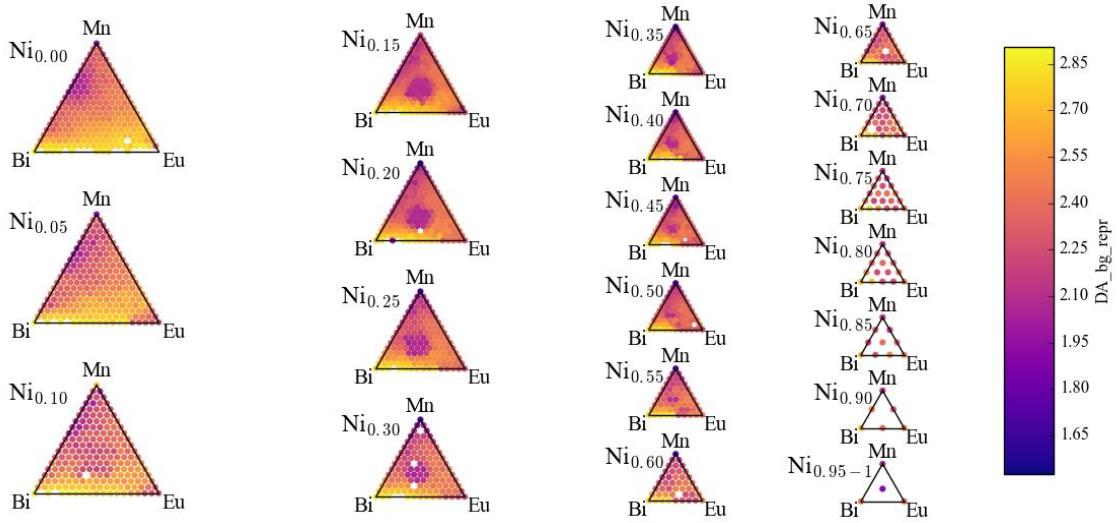

Figure S8(a,b). Physical composition space images (a) and direct allowed band gap (b) of a Bi-Mn-Eu-Ni 5 at.% library.

a

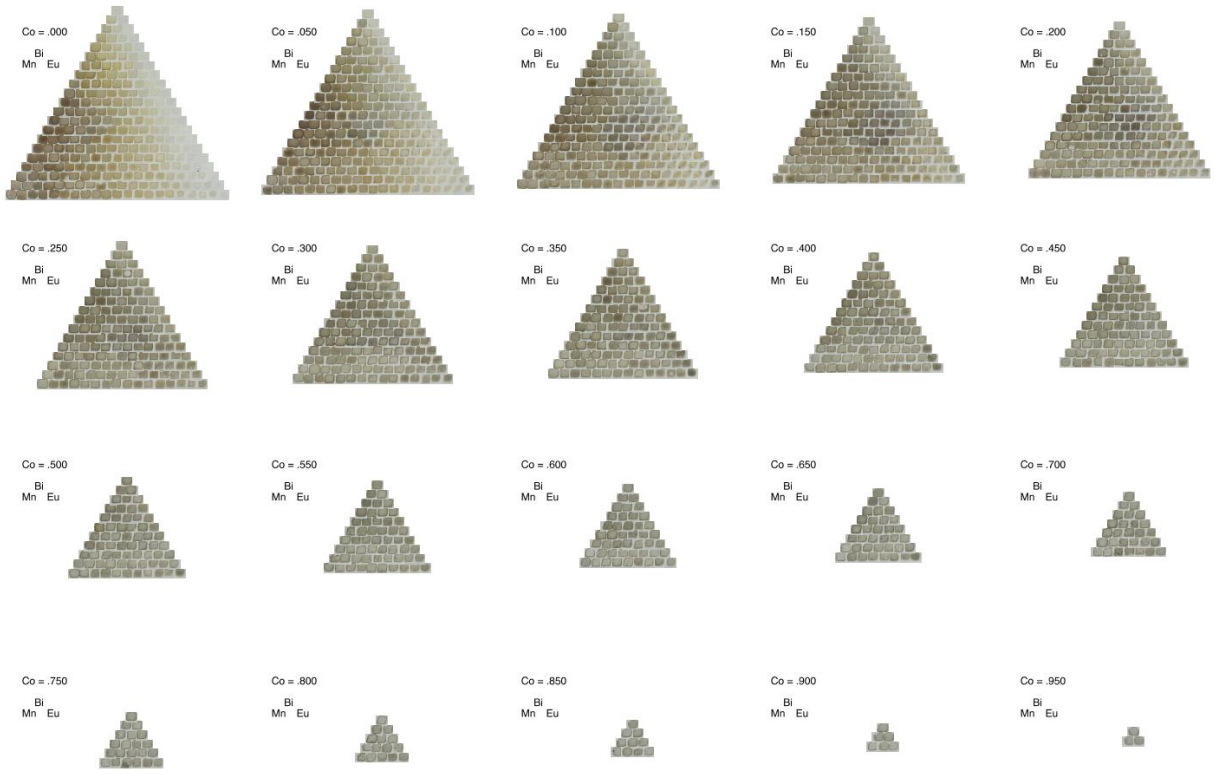

b

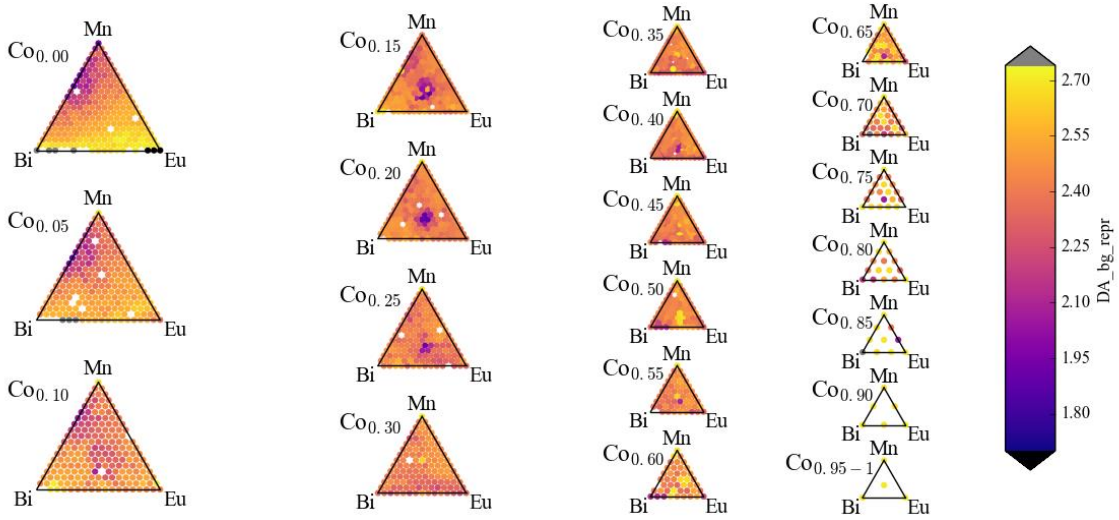

Figure S9(a,b). Physical composition space images (a) and direct allowed band gap (b) of a Bi-Mn-Eu-Co 5 at.% library.

a

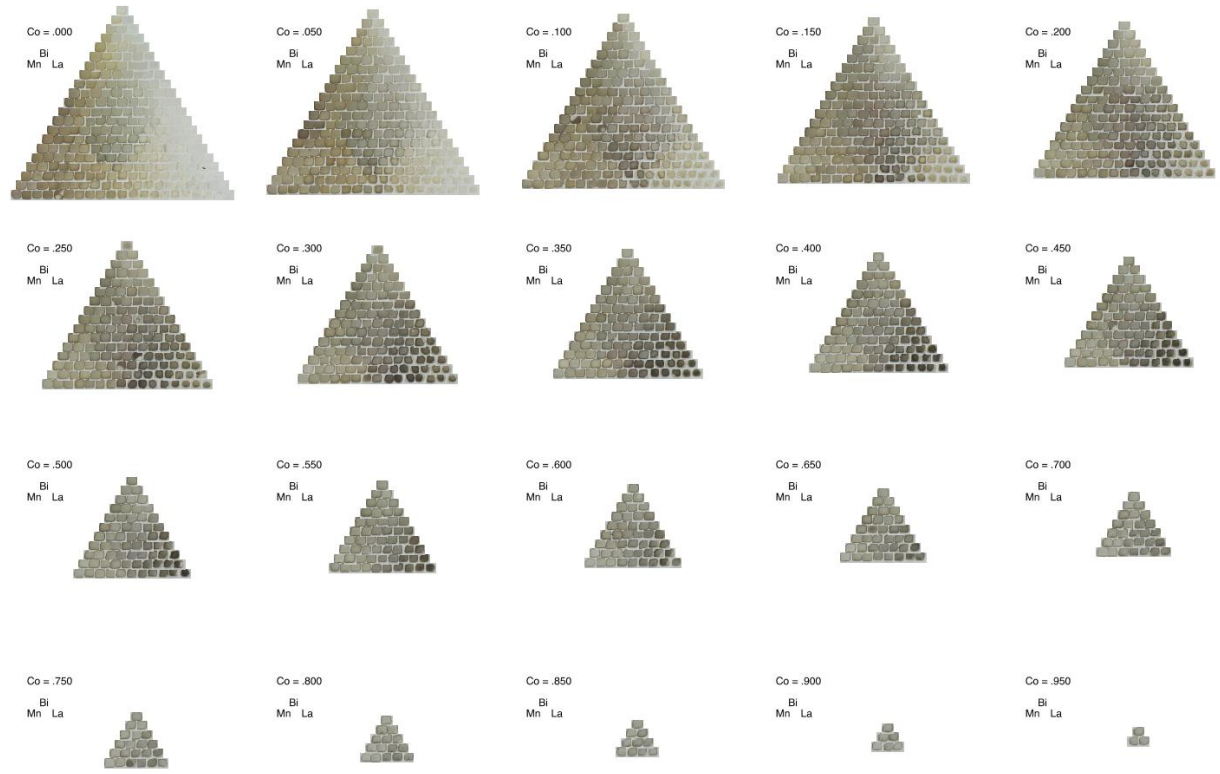

b

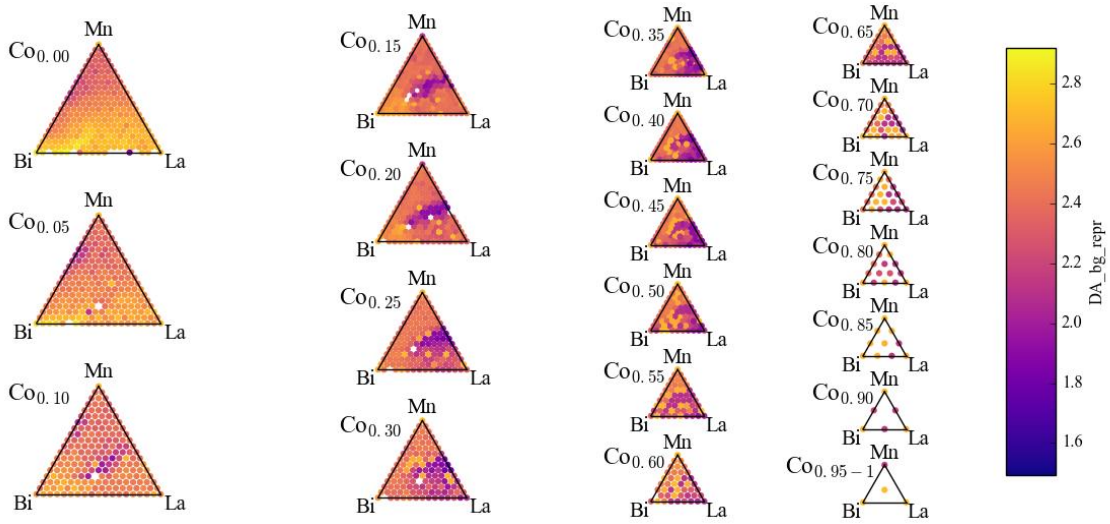

Figure S10(a,b). Physical composition space images (a) and direct allowed band gap (b) of a Bi-Mn-La-Co 5 at.% library on an FTO substrate.

a

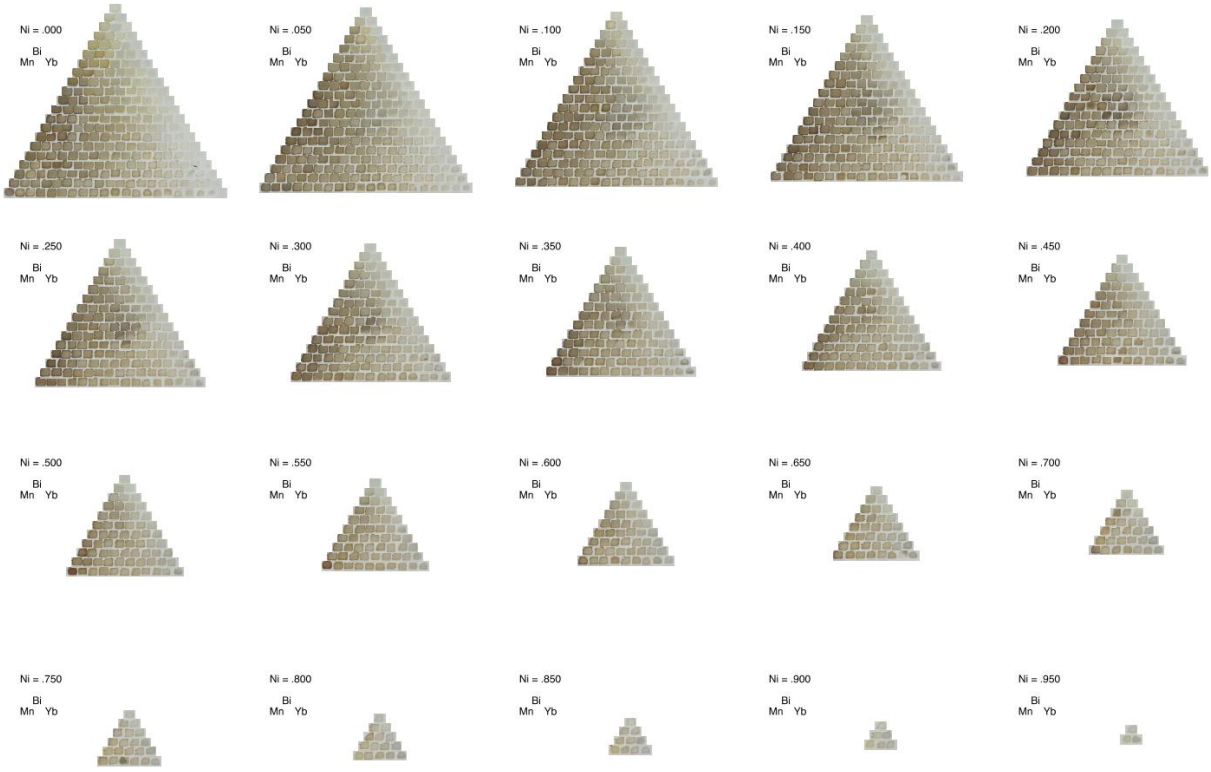

b

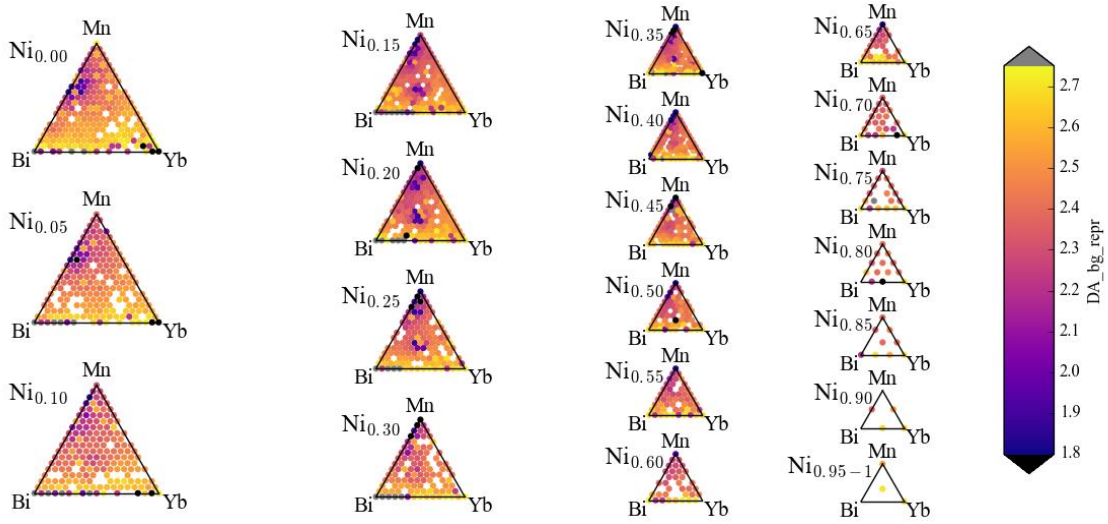

Figure S11(a,b). Physical composition space images (a) and direct allowed band gap (b) of a Bi-Mn-Yb-Ni 5 at.% library on an FTO substrate

a

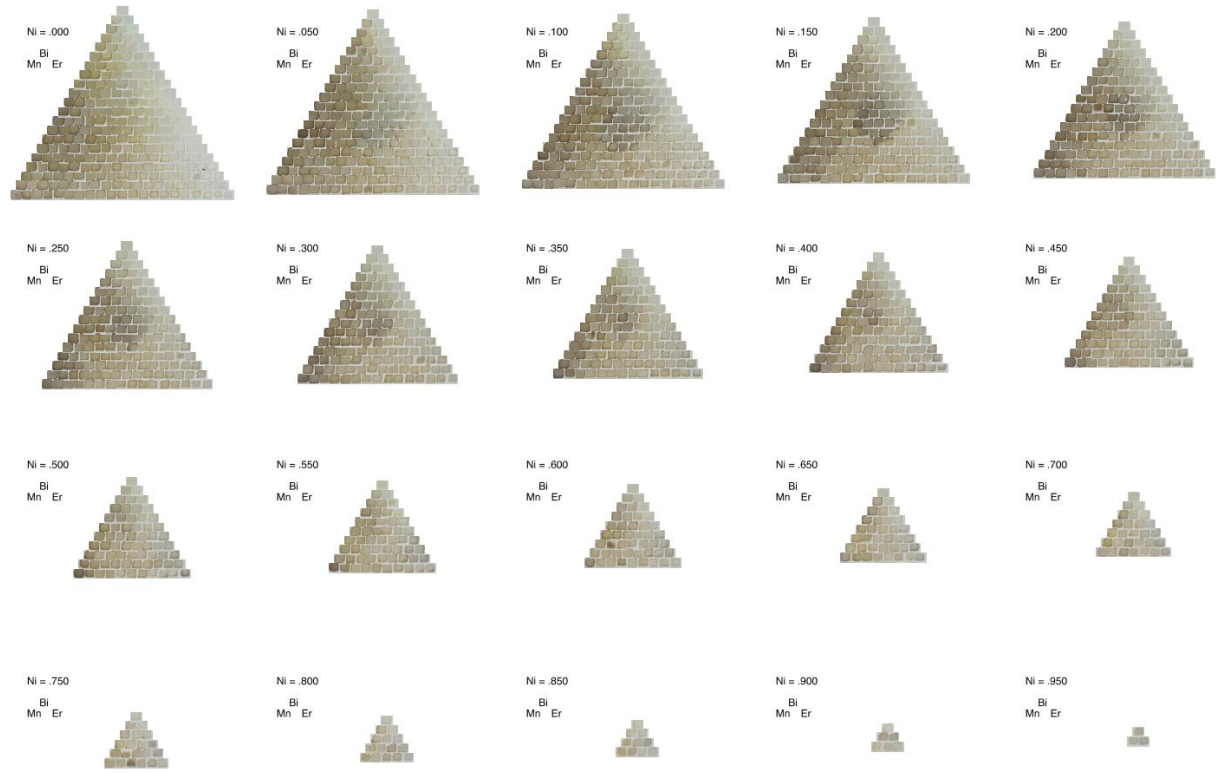

b

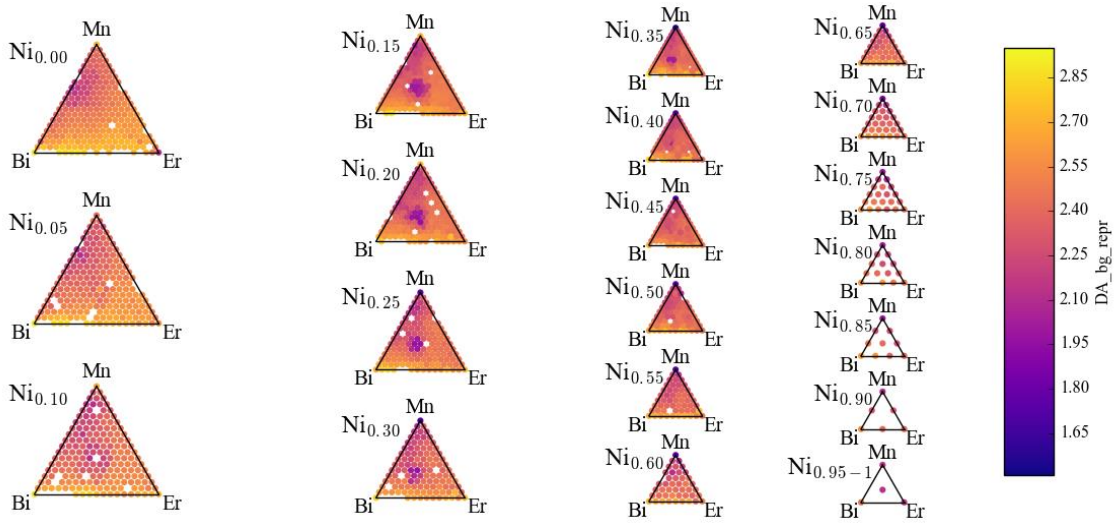

Figure S12(a,b). Physical composition space images (a) and direct allowed band gap (b) of a Bi-Mn-Er-Ni 5 at.% library on an FTO substrate.

a

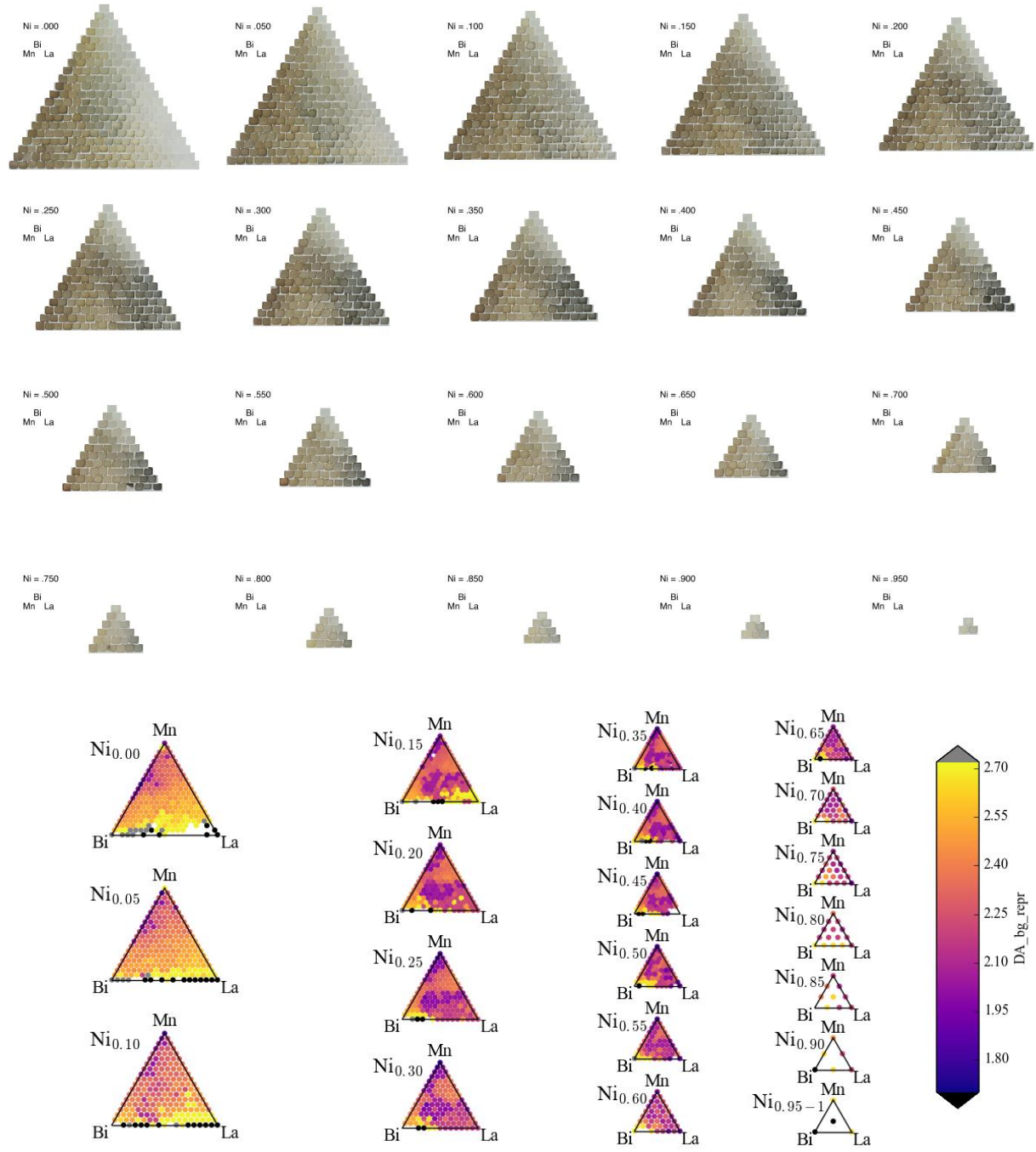

Figure S13(a,b). Physical composition space images (a) and direct allowed band gap (b) of a Bi-Mn-La-Ni 5 at.% library on an FTO substrate.

Note on Tolerance factors

The Goldschmidt tolerance factor, *t*, is an indicator of the stability of the perovskite structure based only on the chemical formula and the ionic radii of each ion:

$$t = \frac{r_A + r_O}{\sqrt{2}(r_B + r_O)}$$

As noted in Ref. [1], for 1.00 > *t* > 0.97 the most likely structure corresponds to the I 4/m tetragonal space group, and finally, if 0.97 > *t* the compound becomes either monoclinic ($P2_1/n$) or orthorhombic.

Using ionic radii from Ref. [2], with extrapolation required to estimate the 12-coordinate radius of Bi^{3+}, we use 12-coordinate radii of 145 pm for Bi^{3+} and 124 pm for Sm^{3+}; 6-coordinate radii of 53 pm for Mn^{4+} and 69 pm for Ni^{2+}; and 2-coordinate radius of 135 pm for O^{2-}.

In the absence of Bi, *t* for $Sm_{0.5}Mn_{0.3}Ni_{0.2}$ is 0.942. When substituting 20% Bi into Sm site, t increases to 0.973. The increase in tolerance factor is indicative of the reduction of the tilting of the octahedral, which is near the upper limit for typical formation of a structure with $P2_1/n$ monoclinic symmetry. This increase in *t* with Bi alloying motivates further study of the influence on distortion including a possible transition to a tetragonal perovskite with increased alloy concentration, and consideration of whether the increase in *t* is related to the solubility limit (at ambient pressure) and/or lowered synthesis temperature compared to the Sm end-member phase.

(1) Serrate, D.; Teresa, J. M. D.; Ibarra, M. R. Double Perovskites with Ferromagnetism above Room Temperature. *J. Phys.: Condens. Matter* **2006**, *19* (2), 023201. https://doi.org/10.1088/0953-8984/19/2/023201.

(2) Shannon, R. D. Revised Effective Ionic Radii and Systematic Studies of Interatomic Distances in Halides and Chalcogenides. *Acta Cryst A* **1976**, *32* (5), 751–767. https://doi.org/10.1107/S0567739476001551.